# Electrical properties tunability of large area MoS<sub>2</sub> thin films by oxygen plasma treatment



Cite as: Appl. Phys. Lett. 116, 223102 (2020); https://doi.org/10.1063/5.0008850 Submitted: 25 March 2020 . Accepted: 25 May 2020 . Published Online: 03 June 2020

Bhim Chamlagain 🔟, and Saiful I. Khondaker 🔟

# COLLECTIONS

This paper was selected as an Editor's Pick







Lock-in Amplifiers up to 600 MHz







# Electrical properties tunability of large area MoS<sub>2</sub> thin films by oxygen plasma treatment @

Cite as: Appl. Phys. Lett. **116**, 223102 (2020); doi: 10.1063/5.0008850 Submitted: 25 March 2020 · Accepted: 25 May 2020 · Published Online: 3 June 2020









Bhim Chamlagain (n) and Saiful I. Khondaker (1,2,a) (n)



# **AFFILIATIONS**

- $^1$ NanoScience Technology Center and Department of Physics, University of Central Florida, Orlando, Florida 32826, USA
- <sup>2</sup>Department of Electrical and Computer Engineering, University of Central Florida, Orlando, Florida 32826, USA

### **ABSTRACT**

MoS<sub>2</sub> thin films prepared via sulfurization of molybdenum films have attracted great attention due to their advantage for scalable synthesis with a large area coverage. However, the MoS2 thin films are typically more resistive than their exfoliated and co-evaporation chemical vapor deposition based counterparts. The ability to modulate the electrical property of MoS<sub>2</sub> thin films will have a significant impact on scalable device applications in electronics, sensors, and catalysis. Here, we report the tuning of electrical transport properties of large area MoS2 thin films with different oxygen plasma exposure times. The electrical transport measurements of the pristine and plasma treated samples reveal that with increasing oxygen plasma treatment, the resistance of the MoS<sub>2</sub> thin films first decreases by almost an order of magnitude and then increases again. The x-ray photoelectron spectroscopy measurements show that the S:Mo ratio continuously decreases with increasing plasma exposure time. For a short plasma exposure time, the resistance decrease can be explained due to the creation of sulfur vacancies leaving unsaturated electrons with molybdenum (Mo) atoms which act as electron donors. With increasing plasma exposure, more sulfur vacancies and hence more Mo atoms are created, many of which get converted to insulating MoO3 resulting in an increase in the resistance of the MoS<sub>2</sub> thin film. The results presented here are a major step forward in realizing the overreaching goals of MoS<sub>2</sub> thin films for practical device applications.

Published under license by AIP Publishing. https://doi.org/10.1063/5.0008850

Two-dimensional (2D) molybdenum disulfide (MoS<sub>2</sub>) has attracted significant attention due to its potential opportunities for designing unique device structures as well as for its potential applications in electronics, optoelectronics, catalysis, sensor, and energy storage devices. <sup>1-8</sup> A majority of the devices are made of mechanically exfoliated flakes from an MoS2 single crystal due to its high crystalline quality with excellent electrical properties. However, this method is not suitable for scalable device fabrication due to the lack of control on the size and thickness of MoS<sub>2</sub> flakes resulting in a poor device yield. Co-evaporation based chemical vapor deposition (CVD) using MoO<sub>3</sub> and sulfur (S) precursors for Mo and S vapors has been used for large scale synthesis of MoS<sub>2</sub> which often yields 10–100 μm size isolated triangles and in some cases continuous films of limited size with non-uniform thickness (mostly a combination of mono and bi-layer regions). 9-11 On the other hand, MoS2 thin films prepared via sulfurization of Mo or MoO3 thin films can be advantageous for scalable device fabrication due to their large area coverage, controlled synthesis in a wide range of thickness, and relatively easier cost-effective synthe-However, thin films of MoS<sub>2</sub> are typically more

resistive than their exfoliated and co-evaporation CVD based counterparts owing to the much smaller grain size, typically in the range of 10-100 nm, which gives rise to significantly more grain boundaries limiting their potential use in practical device applications.<sup>19</sup> In addition, with increasing Mo film thickness, the orientation of MoS<sub>2</sub> layers changes from horizontal to vertical.<sup>20</sup> The ability to control the electrical property of the MoS<sub>2</sub> thin films could be significant for many important applications with optimum performance. For example, more resistive samples could be useful for sensors while less resistive samples could be useful for electronics. A useful approach to control the electrical properties of the MoS2 thin films could be via post growth modification. However, tuning the electrical properties of MoS<sub>2</sub> thin films through such an approach is yet to be demonstrated which could open opportunities for scalable device applications in electronics, optoelectronics, catalysis, sensor, energy storage, and piezoelectric devices.

Here, we present a general strategy to tune the electrical properties of MoS<sub>2</sub> thin films via oxygen plasma treatment with different exposure times. The MoS<sub>2</sub> thin films were prepared via low pressure

a) Author to whom correspondence should be addressed: saiful@ucf.edu

sulfurization of the molybdenum film. We carried out electrical transport measurements of MoS2 devices and found that the resistance of the MoS<sub>2</sub> device decreases by an order of magnitude with a short oxygen plasma exposure time, but the long exposure of the plasma increases the resistance of the sample. X-ray photoelectron spectroscopy (XPS) measurements show a change of the sulfur to molybdenum ratio and formation of molybdenum oxides with plasma exposure time. For a short plasma exposure time, the sulfur to molybdenum ratio of the MoS2 sample decreases compared to the pristine sample suggesting the formation of sulfur vacancies. The creation of sulfur vacancies leaves molybdenum with unsaturated electrons which act as electron donors. This will cause the increase in electronic carriers to the MoS<sub>2</sub> device and decrease the resistance of the sample. For the long plasma exposed sample, the formation of MoO3 was observed. The insulating nature of the formed oxide increases the resistance of the MoS<sub>2</sub> film. With further increase in the plasma exposure time, the amount of MoO3 also increases resulting in the formation of MoO<sub>3</sub> patches which further increases the resistance of the thin

The MoS<sub>2</sub> thin film was grown via low pressure sulfurization of the molybdenum (Mo) film inside a horizontal tube furnace equipped with a 1-in. quartz tube. An Mo film of 6 nm thickness was deposited on a Si/SiO<sub>2</sub> substrate (250 nm thick thermal oxide layer) via electron beam evaporation. The substrate was placed in the center zone of the furnace and pumped down to a base pressure of ~30 mTorr. The chamber was then purged with argon (Ar) gas at 130 standard cubic centimeter per minute (sccm) for the removal of any residual oxygen and water vapor. The furnace was then heated to the growth temperature of 800 °C at a ramping rate of 15°/min and was maintained at that temperature for 55 min. Sulfur (S) powder was placed at the upstream side of the furnace so that Ar gas can carry the S vapor to the central zone of the furnace for the sulfurization process. After the growth, the chamber was allowed to cool to room temperature naturally. Figure 1(a) shows a digital image of an Mo film while Fig. 1(b) shows a digital image of the same film after sulfurization. The change

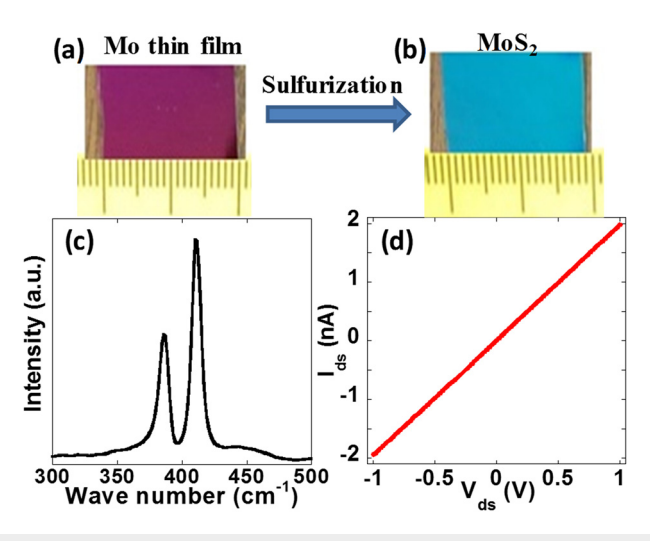


**FIG. 1.** Digital images of (a) Mo and (b) large area MoS<sub>2</sub> films prepared after low pressure sulfurization of Mo. (c) Raman spectrum of the pristine MoS<sub>2</sub> thin film. (d) Current–voltage (I–V) characteristics of a representative pristine MoS<sub>2</sub> device.

of color indicates the Mo film was sulfurized to MoS<sub>2</sub>. The final MoS<sub>2</sub> thickness is expected to increase by about 2-3 times that of the initial metal thickness and the layers are expected to be vertically oriented. 16,17,20 Raman spectroscopy was used to confirm that the prepared film was MoS<sub>2</sub> [Fig. 1(c)]. The Raman spectra show two prominent peaks at 386.1 cm<sup>-1</sup> and 411.1 cm<sup>-1</sup>, corresponding to the in-plane  $E_{2g}^{1}$  and out of plane  $A_{1g}$  vibrational peaks, respectively, with a position difference of 25.0 cm<sup>-1</sup>, consistent with the reported values of MoS<sub>2</sub> films prepared by a similar method. <sup>21–25</sup> For electrical transport characterization, MoS<sub>2</sub> devices of 100 µm channel length and 300  $\mu$ m channel width were fabricated by depositing 5 nm/35 nm of Cr/Au using a shadow mask. Electrical transport measurements were performed on a probe station in an ambient condition using a Keithley 2400 source meter and a DL instrument 1211 current preamplifier interfaced with the LabView program. Figure 1(d) shows the current-voltage (I-V) characteristics of a representative MoS<sub>2</sub> device. We have used highly doped Si as a back gate, however, no gate dependence was observed similar to what has been reported in a few other reports<sup>4,20,26</sup> probably due to the vertical orientation of the layers. The resistance calculated from the linear region of the I-V curve was found to be 509 M $\Omega$ . We have measured a total of 27 MoS<sub>2</sub> devices that were fabricated on the same chip and the resistance varies from 475.0 M $\Omega$  to 540.0 M $\Omega$  with an average of 500 M $\Omega$ . This is consistent with the reported resistance value of the MoS<sub>2</sub> film prepared by a sim-

All the samples were then treated in an oxygen plasma chamber for various times (10 s-30 min) and the transport measurements were repeated after each oxygen plasma treatment. The plasma treatment was carried out using a commercial (Plasma Etch, PE50) plasma chamber at a power of 25 W operating at 50 kHz. During plasma exposure, the pressure within the plasma chamber was held at 200-250 mTorr and a gas mixture of oxygen (20%) and argon (80%) was passed at a constant rate of 15 sccm. The total plasma exposure time at a given step is the sum of all previous step(s) exposure time plus additional exposure time of that step. Figure 2(a) shows the I-V characteristics of the same MoS2 device that was presented in Fig. 1(d), after different oxygen plasma exposure times. The resistance was calculated from the linear fit of the I-V curve. After first plasma treatment (10 s), the resistance of the sample significantly decreased to 191 M $\Omega$ . After an additional 20 s plasma treatment (total 30 s), the resistance further decreased to 115 M $\Omega$ . The resistance continued to decrease to 59 M $\Omega$  for 1 min, 43 M $\Omega$  for 2 min, and 37 M $\Omega$  for 5 min plasma exposure. We observed that the resistance continuously decreased with increasing plasma exposure time until 5 min. Interestingly, after 10 min of plasma exposure, the resistance started to increase. For instance, the resistance of the  $MoS_2$  device was 66  $M\Omega$ , 377 M $\Omega$ , and 1.02 G $\Omega$  for 10 min, 20 min, and 30 min plasma exposure times, respectively. We have measured all the 27 MoS<sub>2</sub> devices after different plasma exposure times, and a similar trend of resistance variation was observed. This trend is clearly shown in Fig. 2(b) where we present the box plot of resistance at each plasma exposure time. It is clearly seen that the average resistance of all the samples decreases at first with a short oxygen plasma exposure time, remains almost constant at intermediate exposure and eventually increases with a long enough plasma exposure time (above 15 min).

To explore the physical mechanism responsible for the observed changes in the electronic transport properties, we performed x-ray

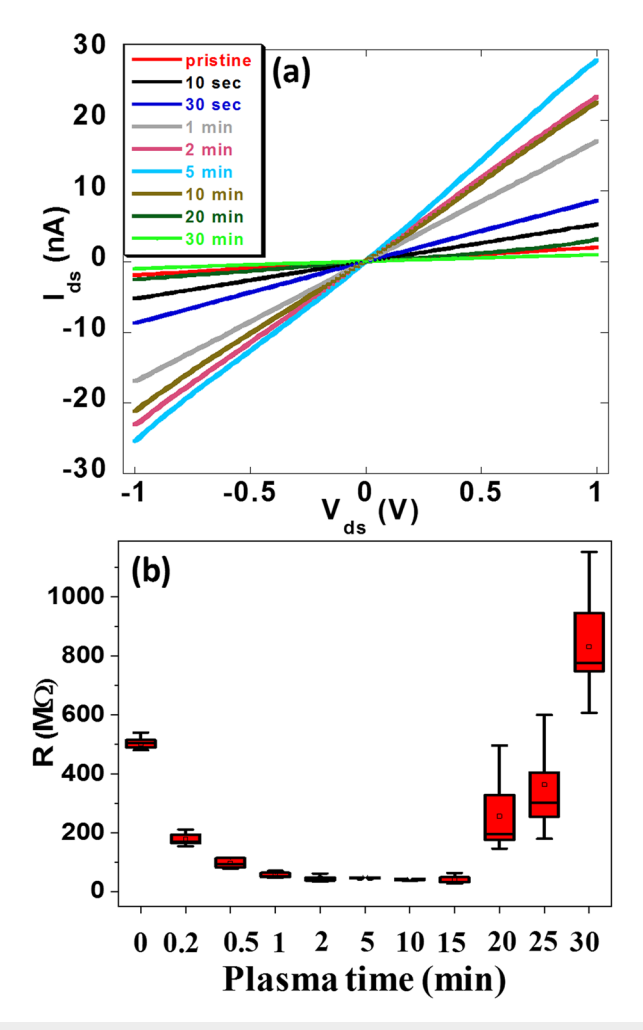


**FIG. 2.** (a) I–V characteristics of a representative  $MoS_2$  device with different plasma exposure times. (b) Statistics of resistance variation of  $MoS_2$  devices with different plasma exposure times.

photoelectron spectroscopy (XPS) on the pristine and plasma treated MoS<sub>2</sub> samples. XPS measurements were performed using a Thermo Scientific (Escalab Xi) XPS system with a monochromatic Al  $K\alpha$  radiation source. MoS<sub>2</sub> samples were prepared and treated with oxygen plasma right before XPS measurement to minimize the ambient exposure effect. A pass energy of 20 eV with a 0.1 eV scanning step was used for photoelectron detection. XPS spectra were recorded onto the sample surface with a scan area of 300  $\times$  300  $\mu$ m<sup>2</sup>. The carbon (C) 1s reference line at the binding energy of 284.8 eV was used to calibrate the charging effect. Figure 3 shows the experimental data (open symbols) and convoluted spectra for the pristine, 1 min (when resistance significantly decreases), 5 min (when resistance becomes minimum and flat), and 30 min (resistance increases to the highest value) plasma treated MoS<sub>2</sub> samples. Figure 3(a) presents the Mo 3d core level XPS spectra of the pristine MoS<sub>2</sub> film. The convoluted spectra show three prominent peaks at 226.0, 228.9, and 232.0 eV which correspond to binding energies (BEs) of S 2s, Mo<sup>4+</sup> 3d<sub>5/2</sub>, and Mo<sup>4+</sup> 3d<sub>3/2</sub> electrons of the MoS<sub>2</sub> crystal, respectively. Figure 3(b) shows the S 2p core level

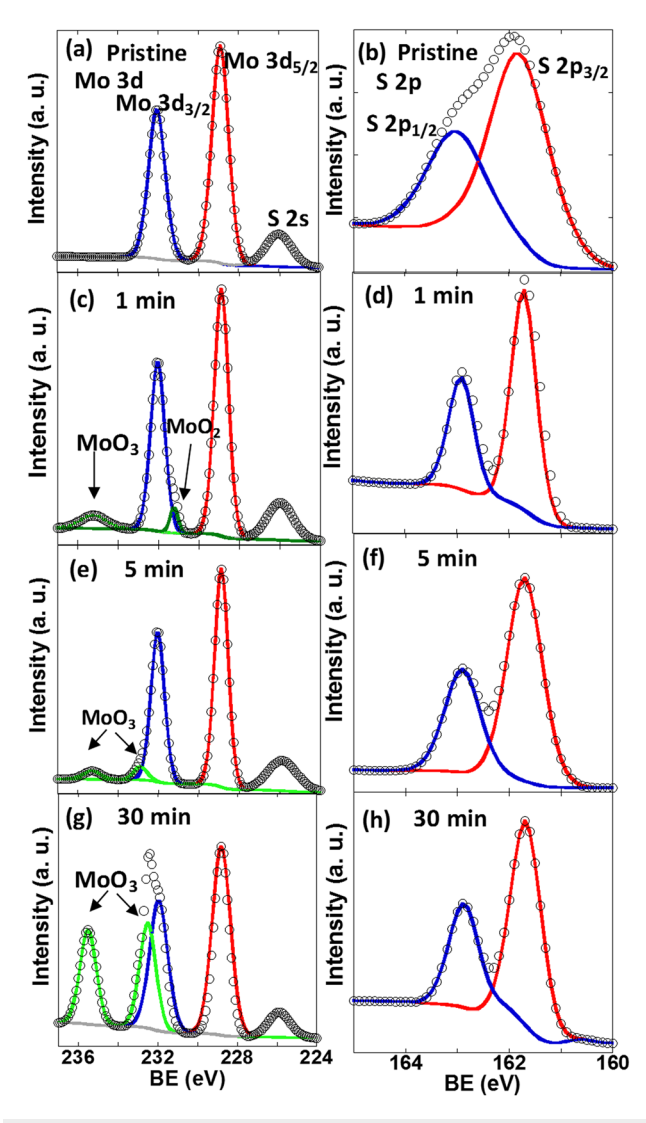


**FIG. 3.** Core levels XPS spectra of the  $MoS_2$  film. (a), (c), (e), and (g) are the Mo 3d core level XPS spectra of the pristine  $MoS_2$  film, after 1 min, 5 min, and 30 min oxygen plasma exposure, respectively. (b), (d), (e), and (h) are the S 2p core level XPS spectra of the pristine  $MoS_2$  film, after 1 min, 5 min, and 30 min oxygen plasma exposure, respectively. The symbols are experimental data. The spectra were convoluted using Gaussian–Lorentzian curves (solid lines).

XPS spectra with peaks at 161.8 and 163.0 eV corresponding to the  $2p_{3/2}$  and  $2p_{1/2}$  spin–orbit split components of MoS<sub>2</sub>, respectively.<sup>29</sup> The ratio of the sulfur to molybdenum was 2.03:1 for the pristine MoS<sub>2</sub> sample and calculated by using the expression S: Mo = A<sub>S</sub>/ (A<sub>Mo4+</sub> + A<sub>Mo6+</sub>), where A<sub>S</sub>, A<sub>Mo4+</sub>, and A<sub>Mo6+</sub> are the atomic percentages of sulfur, Mo<sup>4+</sup>, and Mo<sup>6+</sup>, respectively.

Figure 3(c) shows the Mo 3d core level spectra of the 1 min plasma treated MoS<sub>2</sub> film. In addition to the peaks observed for the pristine sample at the same BEs, two additional peaks at 231.2 and 235.2 eV were observed which correspond to the oxides of molybdenum.<sup>30–33</sup> In some report, the peak at 231.2 was associated with Mo oxysulfide.<sup>34</sup> Figure 3(d) shows the S 2p spectra for 1 min plasma

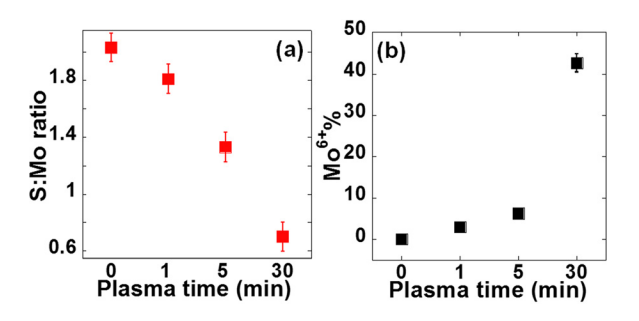


**FIG. 4.** (a) S:Mo ratio of the  $MoS_2$  film with different plasma exposure times. (b) Percentage of  $MoS_2$  transformed into  $MoO_3$  with different plasma exposure times.

treated sample with peaks observed at the same BEs as the pristine sample. Surprisingly, the sulfur to molybdenum ratio decreased to 1.81 compared to the pristine sample. This indicates that the oxygen plasma removes sulfur and creates sulfur vacancies which decreases the sulfur to molybdenum ratio.

The core level spectra of Mo and S for the 5 min plasma treated MoS<sub>2</sub> film are presented in Figs. 3(e) and 3(f), respectively. All the peaks corresponding to Mo 3d, S 2s, and S 2p were found at the same BEs of the pristine MoS<sub>2</sub> film, and an additional peak was observed at a binding energy of 235.3 eV which corresponds to the Mo<sup>6+</sup> peak due to the formation of MoO<sub>3</sub> in the MoS<sub>2</sub> film. The percentage of MoS<sub>2</sub> transformed into MoO<sub>3</sub> was 6.2% and was calculated from the area under the MoO<sub>3</sub> peak using the expression: A(MoO<sub>3</sub>)/[A(MoO<sub>3</sub>) + A(MoS<sub>2</sub>)] x 100%, where A(MoO<sub>3</sub>) and A(MoS<sub>2</sub>) are the areas under MoO<sub>3</sub> and MoS<sub>2</sub> of XPS spectra, respectively. We also calculated the S:Mo ratio to further decrease to 1.33 for the 5 min plasma treated MoS<sub>2</sub> film.

Figures 3(g) and 3(h) represent the XPS spectra of the 30 min plasma treated MoS<sub>2</sub> sample. Interestingly, the Mo<sup>6+</sup> peaks became more prominent although all the peaks corresponding to the pristine MoS<sub>2</sub> film were also found. The significantly increased intensity of the Mo<sup>6+</sup> peak suggests that a large amount of MoS<sub>2</sub> was converted into MoO<sub>3</sub>. The amount of MoS<sub>2</sub> transformed into MoO<sub>3</sub> was calculated from the area under the MoO<sub>3</sub> curve and found to be 43%. These results confirm progressive oxidation over the plasma exposure time. Additionally, the S:Mo ratio for the 30 min plasma treated MoS<sub>2</sub> was calculated to be 0.70.

The variations of the S to Mo ratio and percentage of  $MoO_3$  formation are clearly presented in Figs. 4(a) and 4(b), respectively. The

S to Mo ratio decreased by 15% with initial 1 min plasma exposure to the MoS<sub>2</sub> film. On the other hand, 3% of the MoS<sub>2</sub> was converted to MoO<sub>3</sub> with initial 1 min plasma exposure which increased to 6% with 5 min plasma treatment. Remarkably, the formation of MoO<sub>3</sub> was significantly increased to 43% with 30 min plasma exposure time. The formation of S vacancies (and creation of MoO<sub>3</sub>) is also consistent with Raman measurements where we observed a decrease in intensity and broadening of E<sup>1</sup><sub>2g</sub> and A<sub>1g</sub> peaks with increasing plasma exposure time (see the supplementary material) signifying lattice distortion in  $MoS_2$ .<sup>35</sup> In addition, we observed weak Raman peaks at 223 and 284.7 cm<sup>-1</sup> for pristine and 1 min plasma treated samples. For the 30 min sample, we observed an additional peak at 200 cm<sup>-1</sup> with the peak intensity at 223 cm<sup>-1</sup> remaining unchanged while the peak at 284.7 cm<sup>-1</sup> becomes more prominent. All these peak positions coincide with the MoO<sub>3</sub> Raman peaks.<sup>36</sup> However, the peaks at 223 cm<sup>-1</sup> have also been associated with Mo oxysulfide by some authors.<sup>29,37</sup> This along with the presence of the Mo  $3d_{5/2}$  doublet with a BE of 231.2 eV in XPS for the 1 min plasma treated sample, suggests that we cannot completely rule out Mo oxysulfide in the 1 min plasma treated sample. However, for a longer plasma exposure time, we rule out the presence of Mo oxysulfide as no peak at 231.2 eV was observed in XPS.3

Based on the XPS and Raman study, we propose the following qualitative picture (depicted in Fig. 5) to describe the resistance variation of the MoS<sub>2</sub> film with the plasma exposure time. With initial exposure of the oxygen plasma to the pristine MoS<sub>2</sub> film [Fig. 5(a)], the energetic plasma removes S atoms from the MoS<sub>2</sub> lattice creating sulfur vacancies some of which get converted to MoO<sub>3</sub> [Fig. 5(b)] and possibly some to Mo oxysulfide as well. The existence of S vacancies in MoS<sub>2</sub> has been studied before and it was found that mono-S vacancies are the most abundant. 38,39 The creation of S vacancies leaves Mo atoms with unsaturated electrons which act as electron donors.<sup>40</sup> This causes an increase in the electron concentration and hence a decrease in the resistance of the MoS2 film. Some studies suggested that the formation of the S-O bond in an MoS2 flake with oxygen plasma treatment decreases the resistance of the sample.<sup>31,43</sup> We did not observe S-O (164.8 eV)<sup>44,45</sup> bond formation which rule out the case. With further increase in the plasma exposure time, more sulfur vacancies are created leaving more unsaturated Mo atoms and more MoO<sub>3</sub> gets created. This process continuous and MoO<sub>3</sub> patches are formed in the MoS<sub>2</sub> film with a longer plasma exposure. Since MoO<sub>3</sub> is insulating in nature, there is a competition between electron donating Mo atoms and insulating MoO<sub>3</sub> at intermediate plasma exposure

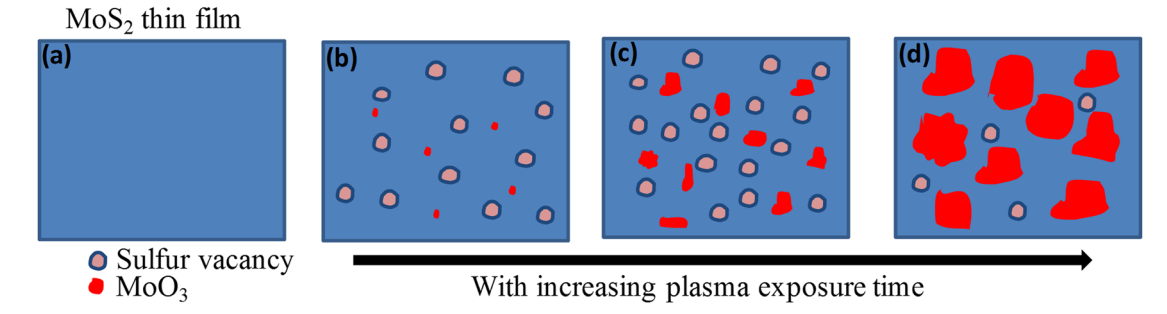


FIG. 5. Schematic diagram illustrating the effect of oxygen plasma on the MoS2 thin film. With increasing plasma exposure time, sulfur vacancies and insulating MoO<sub>3</sub> domains are formed in the MoS<sub>2</sub> thin film resulting in a decrease in resistance with a short plasma exposure duration and then an increase in resistance for a long plasma exposure.

and the resistance of the MoS<sub>2</sub> device remains almost constant for 2–15 min of the plasma exposure time. However, with a long enough plasma exposure time, the formation of MoO<sub>3</sub> patches dominates causing an increase in the resistance of the MoS<sub>2</sub> film.

In conclusion, we show that the electrical transport properties of the large area  $MoS_2$  thin film, prepared via low pressure sulfurization of the Mo film, initially decrease by an order of magnitude and then increase again with increasing oxygen plasma exposure time. The XPS study shows that with mild plasma exposure, Mo:S decreases without any significant formation of  $MoO_3$ . With long plasma exposure, Mo:S further decreases with significant formation of  $MoO_3$ . We explain the decrease in resistance due to the donation of electrons by Mo atoms while the resistance increase is due to the formation of insulating  $MoO_3$  patches in the  $MoS_2$  film with long exposure of oxygen plasma.

See the supplementary material for (a) Raman spectroscopy measurements of pristine and plasma treated MoS<sub>2</sub> films.

This work was supported by the U.S. National Science Foundation (NSF) under Grant No. 1728309. We acknowledge Sajeevi Withanage and Professor Laurene Tetard for the help with Raman measurement.

### **DATA AVAILABILITY**

The data that support the findings of this study are available from the corresponding author upon reasonable request.

### **REFERENCES**

- <sup>1</sup>O. Lopez-Sanchez, D. Lembke, M. Kayci, A. Radenovic, and A. Kis, Nat. Nanotechnol. **8**, 497 (2013).
- <sup>2</sup>D. Voiry, M. Salehi, R. Silva, T. Fujita, M. Chen, T. Asefa, V. B. Shenoy, G. Eda, and M. Chhowalla, Nano Lett. 13, 6222 (2013).
- <sup>3</sup>W. Wu, L. Wang, Y. Li, F. Zhang, L. Lin, S. Niu, D. Chenet, X. Zhang, Y. Hao, T. F. Heinz, J. Hone, and Z. L. Wang, Nature **514**, 470 (2014).
- <sup>4</sup>T. Jarvinen, G. S. Lorite, J. Perantie, G. Toth, S. Saarakkala, V. K. Virtanen, and K. Kordas, Nanotechnology **30**, 405501 (2019).
- <sup>5</sup>N. Choudhary, C. Li, H.-S. Chung, J. Moore, J. Thomas, and Y. Jung, ACS Nano 10, 10726 (2016).
- <sup>6</sup>Y. Xue, Y. Zhang, Y. Liu, H. Liu, J. Song, J. Sophia, J. Liu, Z. Xu, Q. Xu, Z. Wang, J. Zheng, Y. Liu, S. Li, and Q. Bao, ACS Nano 10, 573 (2016).
- <sup>7</sup>Y. Zhou, C. Zou, X. Lin, and Y. Guo, Appl. Phys. Lett. **113**, 082103 (2018).
- <sup>8</sup>M. Shang, C. Du, H. Huang, J. Mao, P. Liu, and W. Song, J. Colloid Interface Sci. 532, 24 (2018).
- <sup>9</sup>K. K. H. Smithe, C. D. English, S. V. Suryavanshi, and E. Pop, 2D Mater. 4, 011009 (2016).
- <sup>10</sup> J. Y. Chen, W. Tang, B. B. Tian, B. Liu, X. X. Zhao, Y. P. Liu, T. H. Ren, W. Liu, D. C. Geng, H. Y. Jeong, H. S. Shin, W. Zhou, and K. P. Loh, Adv. Sci. 3, 1500033 (2016).
- <sup>11</sup>D. Dumcenco, D. Ovchinnikov, K. Marinov, P. Lazic, M. Gibertini, N. Marzari, O. Lopez-Sanchez, Y. C. Kung, D. Krasnozhon, M. W. Chen, S. Bertolazzi, P. Gillet, A. Fontcuberta i Morral, A. Radenovic, and A. Kis, ACS Nano 9, 4611 (2015).
- A. Fontcuberta i Morral, A. Radenovic, and A. Kis, ACS Nano 9, 4611 (2015).

  12 A. Gurarslan, Y. Yu, L. Su, Y. Yu, F. Suarez, S. Yao, Y. Zhu, M. Ozturk, Y. Zhang, and L. Cao, ACS Nano 8, 11522 (2014).
- <sup>13</sup>E. Cha, M. D. Patel, J. Park, J. Hwang, V. Prasad, K. Cho, and W. Choi, Nat. Nanotechnol. 13, 337 (2018).
- <sup>14</sup>Y. C. Lin, W. Zhang, J. K. Huang, K. K. Liu, Y. H. Lee, C. T. Liang, C. W. Chu, and L. J. Li, Nanoscale 4, 6637 (2012).

- <sup>15</sup>S. Vangelista, E. Cinquanta, C. Martella, M. Alia, M. Longo, A. Lamperti, R. Mantovan, F. B. Basset, F. Pezzoli, and A. Molle, Nanotechnology 27, 175703 (2016).
- 16N. Choudhary, J. Park, J. Y. Hwang, and W. Choi, ACS Appl. Mater. Interfaces 6, 21215 (2014).
- <sup>17</sup>D. Kong, H. Wang, J. J. Cha, M. Pasta, K. J. Koski, J. Yao, and Y. Cui, Nano Lett. 13, 1341 (2013).
- <sup>18</sup>H. Simchi, T. N. Walter, T. H. Choudhury, L. Y. Kirkley, J. M. Redwing, and S. E. Mohney, J. Mater. Sci. **52**, 10127 (2017).
- <sup>19</sup>H. J. Kim, H. Kim, S. Yang, and J. Y. Kwon, Small **13**, 1702256 (2017).
- 20Y. Jung, J. Shen, Y. Liu, J. M. Woods, Y. Sun, and J. J. Cha, Nano Lett. 14, 6842 (2014).
- <sup>21</sup>H. Li, Q. Zhang, C. C. R. Yap, B. K. Tay, T. H. T. Edwin, A. Olivier, and D. Baillargeat, Adv. Funct. Mater. 22, 1385 (2012).
- <sup>22</sup>C. Lee, H. Yan, L. E. Brus, T. F. Heinz, J. Hone, and S. Ryu, ACS Nano 4, 2695 (2010).
- <sup>23</sup>S. L. Li, H. Miyazaki, H. Song, H. Kuramochi, S. Nakaharai, and K. Tsukagoshi, ACS Nano 6, 7381 (2012).
- <sup>24</sup>S. H. Baek, Y. Choi, and W. Choi, Nanoscale Res. Lett. **10**, 388 (2015).
- <sup>25</sup>D. H. Cho, W. J. Lee, J. H. Wi, W. S. Han, S. J. Yun, B. Shin, and Y. D. Chung, Phys. Chem. Chem. Phys. **20**, 16193 (2018).
- 26T. Momose, A. Nakamura, M. Daniel, and M. Shimomura, AIP Adv. 8, 025009 (2018).
- <sup>27</sup>M. A. Islam, J. Church, C. Han, H. S. Chung, E. Ji, J. H. Kim, N. Choudhary, G. H. Lee, W. H. Lee, and Y. Jung, Sci. Rep. 7, 14944 (2017).
- <sup>28</sup>N. Choudhary, J. Park, J. Y. Hwang, H. S. Chung, K. H. Dumas, S. I. Khondaker, W. Choi, and Y. Jung, Sci. Rep. 6, 25456 (2016).
- <sup>29</sup> A. T. Neal, R. Pachter, and S. Mou, Appl. Phys. Lett. **110**, 193103 (2017).
- <sup>30</sup>S. I. Khondaker and M. R. Islam, J. Phys. Chem. C **120**, 13801 (2016).
- <sup>31</sup>J. Jadwiszczak, C. O'Callaghan, Y. Zhou, D. S. Fox, E. Weitz, D. Keane, C. P. Cullen, I. O'Reilly, C. Downing, A. Shmeliov, P. Maguire, J. J. Gough, C. McGuinness, M. S. Ferreira, A. L. Bradley, J. J. Boland, G. S. Duesberg, V. Nicolosi, and H. Zhang, Sci. Adv. 4, eaao5031 (2018).
- <sup>32</sup>H. Zhu, X. Qin, L. Cheng, A. Azcatl, J. Kim, and R. M. Wallace, ACS Appl. Mater. Interfaces 8, 19119 (2016).
- <sup>33</sup>J. Wang, J. Dong, Y. Xue, X. Yan, and Q. Wang, Appl. Surf. Sci. 495, 143486 (2019).
- <sup>34</sup>T. Weber, J. C. Muijsers, J. H. M. C. van Wolput, C. P. J. Verhagen, and J. W. Niemantsverdriet, J. Phys. Chem. **100**, 14144 (1996).
- <sup>35</sup>N. Kang, H. P. Paudel, M. N. Leuenberger, L. Tetard, and S. I. Khondaker, J. Phys. Chem. C 118, 21258 (2014).
- <sup>36</sup>T. Siciliano, A. Tepore, E. Filippo, G. Micocci, and M. Tepore, Mater. Chem. Phys. 114, 687 (2009).
- Frys. 114, 687 (2009).
   S. Najmaei, Z. Liu, W. Zhou, X. L. Zou, G. Shi, S. D. Lei, B. I. Yakobson, J. C.
- Idrobo, P. M. Ajayan, and J. Lou, Nat. Mater. 12, 754 (2013).
  W. Zhou, X. Zou, S. Najmaei, Z. Liu, Y. Shi, J. Kong, J. Lou, P. M. Ajayan, B. I. Yakobson, and J. C. Idrobo, Nano Lett. 13, 2615 (2013).
- 39J. Hong, Z. Hu, M. Probert, K. Li, D. Lv, X. Yang, L. Gu, N. Mao, Q. Feng, L. Xie, J. Zhang, D. Wu, Z. Zhang, C. Jin, W. Ji, X. Zhang, J. Yuan, and Z. Zhang, Nat. Commun. 6, 6293 (2015).
- 40 Y. Guo, D. Liu, and J. Robertson, Appl. Phys. Lett. 106, 173106 (2015).
- <sup>41</sup>M. Liu, J. Shi, Y. Li, X. Zhou, D. Ma, Y. Qi, Y. Zhang, and Z. Liu, Small 13, 1602967 (2017).
- <sup>42</sup>D. Pierucci, H. Henck, Z. Ben Aziza, C. H. Naylor, A. Balan, J. E. Rault, M. G. Silly, Y. J. Dappe, F. Bertran, P. Le Fevre, F. Sirotti, A. T. C. Johnson, and A. Ouerghi, ACS Nano 11, 1755 (2017).
- <sup>43</sup>S. Kim, M. S. Choi, D. Qu, C. H. Ra, X. Liu, M. Kim, Y. J. Song, and W. J. Yoo, 2D Mater. 3, 035002 (2016).
- T. H. Su and Y. J. Lin, Appl. Phys. Lett. 108, 033103 (2016).
- <sup>45</sup>A. Azcatl, S. McDonnell, S. K. C, X. Peng, H. Dong, X. Qin, R. Addou, G. I. Mordi, N. Lu, J. Kim, M. J. Kim, K. Cho, and R. M. Wallace, Appl. Phys. Lett. 104, 111601 (2014).